Silica Coated $ZnFe_2O_4$ Nanoparticles as Cathode Catalysts for Rechargeable Lithium-Air Batteries

Melike Sevim Yilmaz,[a] Mustafa Coşkun,*[b] Tansel Şener,[c] and Önder Metin*[d]
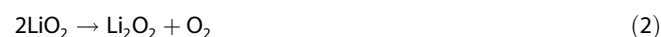
In this work, the preparation and structural characterization of a novel material consisting of silica-coated zinc ferrite ($ZnFe_2O_4$) nanoparticles as cathode catalysts for nonaqueous lithium-air batteries (LABs) are presented for the first time. $ZnFe_2O_4$ nanoparticles (NPs) were prepared by the normal micelles method, using oleic acid as the capping agent and then coating them with silica, via a reverse microemulsion method, with various thicknesses. The colloidal $ZnFe_2O_4$ NPs and silica-coated $ZnFe_2O_4$ NPs were characterized by TEM and powder XRD. The particle size of bare $ZnFe_2O_4$ NPs was calculated to be 5.8 nm by both TEM image and XRD pattern. They were then coated by silica with layer thicknesses of 9, 11, and 13 nm. The perform-ances of bare and silica-coated $ZnFe_2O_4$ NPs were evaluated as cathode catalysts for LABs using 1 M lithium trifluoromethane-sulfonate (TFMS) in tetraethylene glycol dimethyl ether (TEGDME) as the electrolyte. The primary discharge/charge capacities of bare $ZnFe_2O_4$ NPs and $ZnFe_2O_4$ NPs with silica-shell thicknesses of 9, 11, and 13 at 0.1 mA cm^{-2} were found to be 3300, 4300, 6200 and 5000 mAh g^{-1}, respectively. The over-potential is almost 0.5 V, decreased by silica coating with a thickness of 11 nm, whereas there was no difference at other thicknesses. Cyclability with a discharge capacity of 1000 mAh g^{-1} was observed for at least 45 cycles for silica-coated $ZnFe_2O_4$ NPs with a shell thickness of 11 nm.

1. Introduction

Rechargeable batteries, especially lithium-ion batteries (LIBs) have gained a remarkable market success for portable energy storage applications since 90s owing to their long cycle life and high energy efficiency. However, the experts have foreseen that the current specific energy density (250 Wh kg^{-1}) or even the maximum theoretical energy density of LIBs (~300 Wh kg^{-1}) is not enough for electric vehicles (EVs) having driving range of >550 km per one full charge. Moreover, the energy density gap between that of conventional LIBs and the target is large, which indicates the requirement of a new battery system with high energy density and power for EVs applications. In this regard, the lithium-air battery (LAB) system that combines the advan-tages of fuel cell and battery[1] has received wide attention owing to its much higher calculated specific energy density (3,458 Wh kg^{-1}).[2] Although the concept of LABs was proposed by Abraham and Jang in 1996, a practical LAB has not been developed and fabricated yet. There are two types of recharge-able LABs; namely non-aqueous and aqueous. In the non-aqueous LABs, two cell reactions are considered; lithium ion coming from the lithium-source at the anode reacts with

oxygen at the cathode to form lithium oxide (Li_2O), which can be further discharged to form lithium peroxide (Li_2O_2) known as oxygen reduction reaction (ORR) (Eqs: 1–3).[2,3]

$$Li^+ + e^- + O_2 \rightarrow LiO_2 \tag{1}$$

$$2LiO_2 \rightarrow Li_2O_2 + O_2 \tag{2}$$

$$LiO_2 + Li^+ + e^- \rightarrow Li_2O_2 \tag{3}$$

The formed Li_2O_2 is decomposed to Li and O_2 electrochemi-cally, known as oxygen evolution reaction (OER):

$$Li_2O_2 \rightarrow 2Li^+ + 2e^- + O_2 \tag{4}$$

A variety of carbon substrates including carbon nano-tubes,[4] graphene[5] and pyrolytic carbon[6] and/or catalysts[7] have been tested for the cathode of LABs up till now. The surface of the carbon is generally used to store discharge products and to maximize the activity of catalyst for both ORR and OER. The catalyst is used to lower the overpotential associated with the ORR and OER to achieve high specific energy and power. Besides the carbon substrates, much effort has been spent to explore various catalysts such as metal oxides (α-MnO_2, λ-MnO_2, Co_3O_4 and RuO_2.), noble metals (Pt, Au, Ru and Pd) and their alloys (PtNi, PtCo, PtAu and MPd)[8,9,10] for the LAB cathodes till now. Ferrites, a class of metal oxides formed by the reaction of ferric oxide with metals in a spinel crystal structure, have been also studied as cathode catalysts for last five years. For example, we recently reported the cathode performance of 11 nm $CoFe_2O_4$ NPs supported on Vulcan XC-72 at various loadings.[11] The $CoFe_2O_4$@Vulcan with a 16.4 wt% $CoFe_2O_4$ loading provided an initial capacity of 7510 mAh g (Vulcan+$CoFe_2O_4$)$^{-1}$ and 13380 mAh g $CoFe_2O_4^{-1}$ at a current rate of 100 mA g^{-1} in 1 M $LiPF_6$ dissolved in

[a] Dr. M. S. Yilmaz
     Department of Chemistry, Faculty of Science, Atatürk University, Erzurum, Turkey
[b] Dr. M. Coşkun
     Department of Physics Engineering, Hacettepe University, Ankara, Turkey
     E-mail: mcoskun@hacettepe.edu.tr
[c] T. Şener
     KetenciZade Energy, Istanbul, Turkey
[d] Prof. Ö. Metin
     Department of Chemistry, Collage of Sciences, Koç University, 34450 Sarıyer, Istanbul, Turkey
     E-mail: ometin@ku.edu.tr
     An invited contribution to a Special Issue on Bifuctional Catalysis for Metal-Air Batteries

ethylene carbonate and diethyl carbonate mixture (1:1, v/v) as the electrolyte. Li et al[12] reported a specific discharge capacity of 10830 $mAhg^{-1}$ and a long cycling life reaching up to 100 cycles by using ordered mesoporous $NiFe_2O_4$ at a current rate of 0.1 $mAcm^{-2}$ in 1 M $LiCF_3SO_3$-TEGDEM electrolyte. In another study, Guang et al[13] reported that spinel MFe_2O_4 (M= Co, Ni) NPs deposited on multi-walled carbon nanotubes provided the capacity reaching up to 200 $mAhg^{-1}$ using 1 M LITFSI in TEGDME. In a recent study, Sen et al reported very high capacity exceeding 11000 $mAhg^{-1}$ at a current density of 300 mAg^{-1} by using hierarchical mesoporous $ZnO/ZnFe_2O_4/C$ (ZZFC) nanocages as cathode catalysts and 1 M LiTFSI in TEGDME solution as electrolyte at room temperature.[14]

Besides the cathode side, understanding the Li_2O_2 growth/ decomposition mechanism is also very important to improve the capacity and cycle stability of LABs.[15] For instance, Timoshevskii et al[16] demonstrated theoretically that the electronic mobility of Li_2O_2 can be improved by substituting 1.6% of lithium atoms with doped silicon in order to reduce the overall cell resistance and the efficiency of discharge/charge cycles. On the other hand, it was previously reported that silica coated electrode active materials served to improve the electrochemical and thermal properties of lithium-ion[17–20] and lithium-sulfur batteries.[21] Moreover, silica coated separators enhance the ionic conduction wetting and thermal and dimensional stability.[22–25] However, there is only one study using silica for the cathode of LABs at the authors' best knowledge. In this individual study done by Xia and Janek,[26] the addition of 2 wt% silica nanoparticles with a mean particle size of about 7 nm into carbon cathode led to 50% increase of the discharge capacity. Moreover, the charge overvoltage was decreased by 0.2 V, and a cycling performance of 1500 $mAhg^{-1}$ at a current of 100 mAg^{-1} was obtained with 0.5 M $LiSO_3CF_3$-triglyme electrolyte. The authors explained the promoting effect of silica with the prevention of pore clogging of the carbon surface and hence an easier oxygen diffusion into the cathode. In another study, Zhang et al. reported a similar performance enhancement for the Li-ion batteries by using $MHSiO_2@C$ nanocomposites providing a cycling performance up to 500th cycles.[27] These studies along with the other ones reported in the literature revealed that introducing of silica into the cathode of Li-air batteries can enhance the battery performance effectively.[28–33] However, to the best authors' knowledge, there is no example of silica coated MFe_2O_4 NPs as cathode catalysts for the non-aquoues LABs.

In the present study, the electrocatalyst performance of silica coated $ZnFe_2O_4$ NPs was tested for the first time in the cathode of non-aqueous LAB. Oleic acid (OAc) capped $ZnFe_2O_4$ NPs were prepared by using a solvothermal route and coated with silica by reverse microemulsion method at various shell thickness. The cathode performance of silica-coated $ZnFe_2O_4$ NPs was evaluated by studying the galvanostatic discharge/ charge profiles and cycling performance. The effect of the silica layer thickness on the performance of LAB was evaluated as well. A significant enhancement was observed in the discharge capacity (6300 $mAhg^{-1}$ at 0.1 $mAcm^{-2}$) with a silica shell thickness of 11 nm compared to that of uncoated $ZnFe_2O_4$ NPs

(3300 $mAhg^{-1}$ at 0.1 $mAcm^{-2}$) and the $ZnFe_2O_4$ with other shell thickness.

Experimental Section

Synthesis of ZnFe₂O₄ Nanoparticles

Oleic acid (OAc) capped $ZnFe_2O_4$ nanoparticles were prepared by using the method developed by Caruntu et al.[27] In a typical synthesis of OAc-capped $ZnFe_2O_4$ NPs: 4 mmol of $FeCl_3.6H_2O$ (97%), 2 mmol of $ZnCl_2$ (98%) and 70 mL of diethyleneglyol (DEG, 99%) were directly mixed in a three-necked round bottom flask equipped with condenser, magnetic stirrer, thermocouple, heating mantle and stirred under argon atmosphere. In a separate flask, 40 mmol of NaOH (97%) was dissolved in 35 mL of DEG. Next, the NaOH solution was injected into the DEG solution of metal chlorides. After stirring the resultant mixture for 2 h, the mixture was slowly heated to 230°C and kept at this temperature for 2 h. Next, 2.5 mmol of oleic acid (OAc, 95%) was added to the final solution and kept for extra 10 min. After cooling the mixture down to room temperature, the resulting black product was separated by centrifugation at 6000 rpm for 10 min and washed with 20 ml of absolute ethanol (99%) three times and dried under a nitrogen flow.

Silica Coating of ZnFe₂O₄ Nanoparticles

The $ZnFe_2O_4$ NPs were coated with silica by using a well-established water-in-oil microemulsion procedure reported elsewhere.[35] In the protocol, tetraethylorthosilicate (TEOS) was used to coat the $ZnFe_2O_4$ NPs via following a base-catalyzed silica formation around the NPs. Briefly, 8 mL of Igepal CO-520 was mixed with cyclohexane (175 mL) under vigorous stirring at room temperature for 20 min. As-synthesized OAc-functionalized $ZnFe_2O_4$ NPs were dispersed in cyclohexane at a concentration of 1 mg/mL and slowly added to the Igepal CO-520/cyclohexane mixture and well-mixed with Vortex for 3 h. Next, 1.5 mL aqueous ammonia solution (28 wt%) was added dropwise into the mixture and stirred for 5 min. Finally, TEOS was slowly dropped into the mixture. Depending on the desired SiO_2 shell thickness, the amount of added TEOS was varied from 0.5 to 1.5 mL. The coating procedure was proceeded at 30°C for 72 h under vigorously stirring before the addition of ethanol to precipitate the nanoparticles. Finally, silica-coated $ZnFe_2O_4$ NPs were collected by centrifugation and washed at least three times to remove unreacted organic chemicals, and then dried at 30°C for 6 h.

Instrumentation

Transmission electron microscope (TEM) images were obtained on a JEOL JEM-2010F high resolution transmission electron microscope at an accelerating voltage of 200 kV. X-ray powder diffraction (XRD) of the samples were recorded with a EQUINOX 1000 X-ray diffractometer operating with a CoKα source ($\lambda = 0.17902$ nm). FTIR spectrum was recorded on a Bruker Vertex 70v FTIr instrument.

Lithium-Air Battery Tests

As-synthesized silica coated $ZnFe_2O_4$ NPs were mixed with PVDF binder in a weight ratio of 90:10 and well-blended in NMP solution to prepare a catalyst ink. Toray carbon paper was coated by this ink by brush-painting with a loading density of 1.0 ± 0.1 mg.cm^{-2}. Then, the resulting electrodes were dried in a vacuum oven at

130 °C for 12 h. The galvanostatic discharge/charge profiles tests were performed using a homemade cell based on ISO-KF standard high-vacuum components (i.e. sandwich cell). The electrolyte used for this study was composed of 1 M **lithium** trifluoromethanesulfonate (LiTFMS) *in* tetraethylene glycol dimethyl ether (TEGDME) and prepared in a glovebox without exposure to air. 0.1 M potassium iodide was also added to facilitate rechargeability. The cell consisted of a lithium metal disc as anode, a glass-fiber separator (filterLab MFV1, 260 μm thick) soaked with electrolyte, Li metal foil as the anode (Sigma Aldrich, 0.4 mm thick, cut to approx. 0.8 cm^2) and nickel foil served as a current collector. All Li–O$_2$ cells were assembled in an argon-filled glove box. Once assembled, the cell was purged with pure oxygen for several minutes. Electrochemical tests were performed using a Biologic VSP multichannel potentiostat at a potential range between of 2.0 and 4.2 V. All tests were done at room temperature. The battery tests were conducted on an eight channel battery analyzer (MTI Corp.) at a current density of 0.1 mA cm^{-2}.

2. Results and Discussion

2.1. Materials Characterization

The morphology of both OAc-capped and silica coated ZnFe$_2$O$_4$ NPs with various shell thicknesses were characterized by studying their TEM images taken from their ethanol solutions. Figure 1A shows a representative TEM image of OAc-capped colloidal ZnFe$_2$O$_4$ NPs revealing that they have a narrow size distribution with an average size of 5.7 ± 0.7 nm, which is attributed to presence of OAc as capping agent around the surface of ZnFe$_2$O$_4$ NPs. Next, we examined the structure of ZnFe$_2$O$_4$ NPs after the silica coating with the addition of

different amount of TEOS. Figure 1B–D shows the representative TEM images of ZnFe$_2$O$_4$ NPs with the different silica shells depending on the amount of TEOS addition. As clearly be seen by the TEM images, all the ZnFe$_2$O$_4$ NPs were coated with silica shell almost uniformly and there was no agglomerated NPs observed after the silica coating like as initial OAc-capped NPs. Depending on the TEOS amount used in the silica coating process, the NPs with different shell thickness was prepared and the shell thickness of the NPs were calculated to be 9 nm for 0.5 mL TEOS (Figure 1B), 11 nm for 1 mL TEOS (Figure 1C) and 13 nm for 1.5 mL TEOS (Figure 1D) from the TEM images. It can be easily concluded from this results that the shell thickness increases with increasing amount of TEOS. The detailed information about the specific shell thicknesses and ZnFe$_2$O$_4$/silica ratios are summarized in Table 1. As clearly be

Table 1. Several properties of silica-coated ZnFe$_2$O$_4$ NPs.

| TEOS [mL]	Thickness of the silica shell [nm] (from TEM images)	ZnFe$_2$O$_4$ % mass ratio at the cathode	Silica % mass ratio at the cathode
0	0	90	0
0.50	9.2 ± 0.50	7.1	82.9
1.00	11.1 ± 0.57	3	87
1.50	13.0 ± 0.62	2.1	87.9

concluded by the data shown by Table 1, the shell thickness increases by increasing amount of TEOS which is critical in this synthesis protocol as well as for LAB tests (see below).

It should be noted that there were some NPs that remained uncoated when the amount of TEOS lower than 0.5 mL was used in the silica coating while the amounts of TEOS higher than 1.50 mL was used, there was no change observed on the average shell thickness. However, it is observed that the increased amount of TEOS resulted in the formation of hollow spherical silica NPs containing no ZnFe$_2$O$_4$ NPs.

The crystallographic structure of the OAc-capped ZnFe$_2$O$_4$ nanoparticles was identified by powder XRD measurement and the corresponding XRD pattern was presented in Figure 2. The XRD pattern was readily indexed to face centered spinel cubic structure of ZnFe$_2$O$_4$ (JCPDS Card No: 22-1012). No peak belongs to the other zinc oxides structure as the impurity was observed in the XRD pattern indicating the formation of pure ZnFe$_2$O$_4$ phase. The crystallite size was calculated to be 5.9 nm from the XRD pattern using the diffraction peak at $2\theta = 35.1°$ (311) and Scherrer's equation. This value is very close to the one calculated from TEM image (5.7 ± 0.7 nm) indicating the single phase monocrystalline structure of OAc-capped ZnFe$_2$O$_4$ NPs.

2.2. Li-Air Battery Tests and Electrochemical Characterization

The performance of non-aqueous LABs is limited due to the clogging of the porous cathode by insoluble discharge by-products (Li$_2$O$_2$ and LiO$_2$). It was reported that lithium hydroxide (LiOH) is produced at the cathode (Eqn. 5) instead of lithium
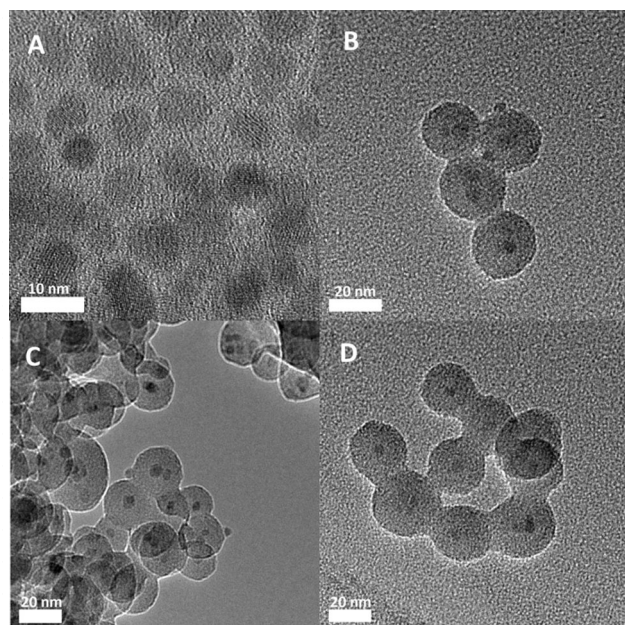
Figure 1. Representative TEM images of ZnFe$_2$O$_4$ NPs: A) OAc-capped; B) silica-coated with a shell thickness of 9 nm (0.5 mL TEOS); C) silica-coated with a shell thickness of 11 nm (1.0 mL TEOS); D) silica-coated with a shell thickness of 13 nm (1.5 mL TEOS).
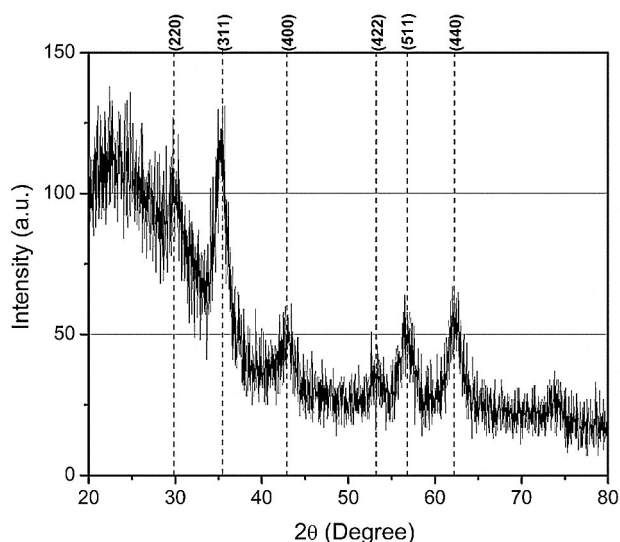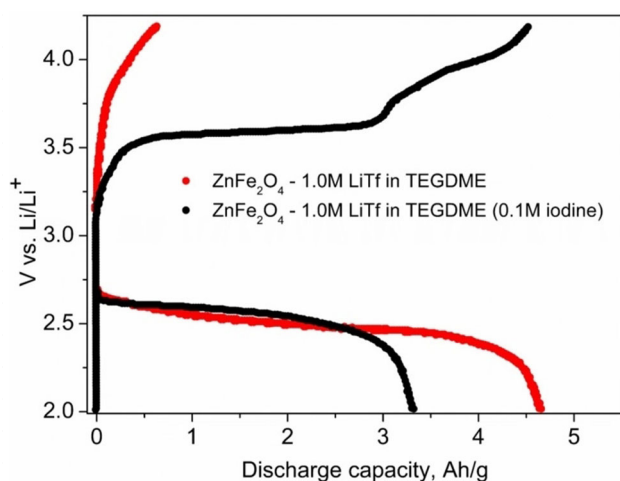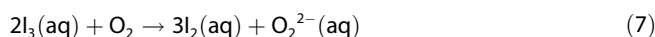
Figure 2. XRD pattern of OAc-capped $ZnFe_2O_4$ NPs.

Figure 3. The discharge/charge profile of an electrode containing OAc-capped $ZnFe_2O_4$ NPs at 0.1 mA.cm^{-2} with and without 0.1 M iodide in the TEGDME electrolyte.

oxides (Eqn. 3 and 4) by the use of redox mediators such as TEMPO[36] and iodine .[37,38]

$$2Li + 1/2O_2 + H_2O \rightarrow 2LiOH \tag{5}$$

In contrast to lithium oxides, LiOH decomposes rapidly when the battery is recharged. Thereby, it becomes possible to recharge LABs at current densities of 0.1 mA cm^{-2}.[35] When the iodine is introduced to the cathode side of the lithium-air battery, it was reported that iodine is firstly reduced at the cathode (Eqn. 6) and subsequently is catalytically re-oxidized by oxygen dissolved in the catholyte (Eqn. 7) to form peroxides and finally peroxides react with Li$^+$ cataion to form Li_2O_2 (Eqn. 8).[39] In this respect, the use of iodine increases the decomposition of Li_2O_2 and thus cycling performance of non-aqueous LABs. However, there was no example of using KI

solution as a co-electrolyte in the literature. Wang et al. investigated iodine doped carbon microspheres and found that iodine ions provide lithium ions attractions by the agency of electronegativity of iodine groups.[40]

$$3I_2(aq) + 2e^- \rightarrow 2I_3^-(aq) \tag{6}$$

$$2I_3^-(aq) + O_2 \rightarrow 3I_2(aq) + O_2^{2-}(aq) \tag{7}$$

$$O_2^{2-} + 2Li^+(aq) \rightarrow Li_2O_2(aq) \tag{8}$$

With considering the aforementioned advantegous of using KI solution as co-electrolyte, we firstly tested the performance of OAc-capped $ZnFe_2O_4$ NPs in the non-aqueous LAB with and without iodine addition into the electrolyte. Figure 3 shows a comparison of discharge/charge profiles of the electrodes comprising OAc-capped $ZnFe_2O_4$ NPs with and without iodine addition into the electrolyte. In the presence of KI co-electrolyte, the average discharging voltage was about 2.75 V while the average charging voltage was about 3.6 V, 0.85 V higher than the discharging voltage. It should be noted that this overpotential value is much better than the cathode catalysts tested in similar Li-air battery systems. In the case of electrolyte without KI addition, although there is no change on the discharging potential (2.7 V), a higher charging voltage (4.2 V) and thus higher overpotential value (1.5 V) is observed. The voltage increases fast towards 4.2 V without iodine. We therefore did not appreciate a significant catalytic activity of OAc-capped $ZnFe_2O_4$ electrode towards the ORR, even if $ZnFe_2O_4$ was expected to be a bifunctional catalyst. However, when iodide is present, the voltage increases more smoothly and forms a plateau at 3.6 V until almost 100 % coulombic efficiency. After this point, voltage increased further possibly with some irreversible oxidative processes involved. On the other hand, besides the overpotential reduction, a decrease on the discharge capacity from ca. 4000 mAh g^{-1} to 3000 mAh g^{-1} is observable in the presence of KI co-electrolyte. These results reveal that KI co-electrolyte addition reduces the ORR performance of OAc-capped $ZnFe_2O_4$ electrode while enhances the OER process.

The discharge/charge profiles of the electrodes containing silica coated $ZnFe_2O_4$ NPs with different shell thicknesses were presented in Figure 4. Although capacities are larger in all cases, they presented a qualitatively similar behavior until almost duplicating the uncoated sample. As it can be seen from the related TEM images, there is no agglomeration when 0.5 mL TEOS is added; 2–3 of $ZnFe_2O_4$ NPs are coated at the same time with a single silica layer. Whereas $ZnFe_2O_4$ particles are coated separetely when the TEOS addition is 1 mL. Additionally, empty silica shells were observed when the TEOS addition is 1.5 mL and the layer thicknesses is increased up to 13 nm. These empty silica shells decrease the capacity of $ZnFe_2O_4$ NPs, because the amount of $ZnFe_2O_4$ NPs which are active cathode catalyst are decreased when TEOS addition reach the 1.5 mL. The highest capacity and the highest hysteresis between discharge/charge profile were provided by the $ZnFe_2O_4$ NPs coated with 11 nm silica shell.
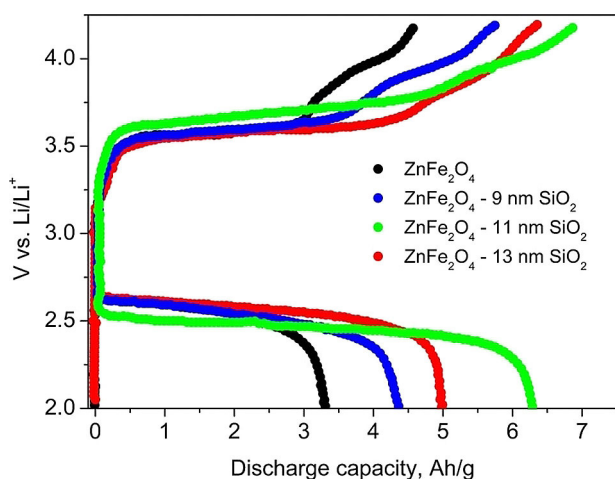
Figure 4. Galvanostatic measurements at 0.1 mA/cm^2 for ZnFe$_2$O$_4$ NPs and silica-coated ZnFe$_2$O$_4$ NPs with layer thicknesses of 9, 11, and 13 nm with 0.1 M iodide in the electrolyte.
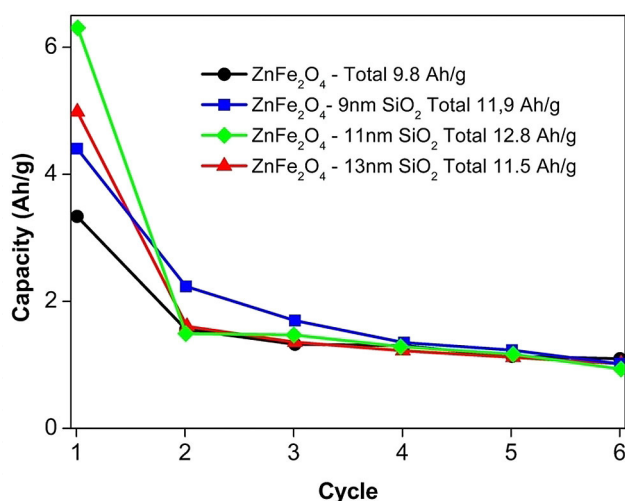
Figure 5. Cycling performance of uncoated and silica-coated ZnFe$_2$O$_4$ NPs with different shell thicknesses.

In other case, the silica nanoparticles kept the porous structure open for oxygen to diffuse deeper into the cathode causing the increase of capacity and rate capability. The nanostructured SiO$_2$ coating film on the surface of particles working as protective layer exhibits higher specific capacity and better rate capability. Particle aggregation may further hinder the electrolyte access to the ZnFe$_2$O$_4$ surface. However, the aggregates may create larger voids in the electrode, which may favor transport through the coated layer, and offer larger space to the discharge products. In effect it seems a more aggregate sample than the others. It also happens that its discharge/charge voltage hysteresis is larger than in all other cases, and the capacity is maximum.

Next, we examined the cycle life of the electrodes containing uncoated and silica coated ZnFe$_2$O$_4$ NPs. All the samples showed a similar cycle life. These results might be explained by originating the similar catalytic systems from the

literature as the following; the initial discharge capacity of a LAB is directly related to the ORR activity of the tested catalysts as it can be clearly understood by the cathode reaction mechanism of the LAB. After a few full capacity discharge cycles, the capacities converge to the same value of about 1000 mAh g^{-1} (Figure 5). In our opinion, we might explain the results not with the nature of the materials itself, but with the aggregation formed by silica coating that generates aggregates in the intermediate sample. Moreover, after the silica coating of nanoparticles, the morphology is changed as well. Super P is a binder which is a highly conductive material compared to silica. In the electrode morphology, this creates the largest regions where SuperP cannot be easily compacted. These volumes can better accomodate Li$_2$O$_2$ deposits. The different discharge voltage might be related to a less homogenous deposit of the SuperP electrode, caused by these larger aggregates. (Figure 5).

Indeed, we obtained at least 45 cycles with a discharge capacity limited to 1000 mAh g^{-1} by using ZnFe$_2$O$_4$ NPs coated with 11 nm silica shell (Figure 6). We believe that the ORR performance of the ZnFe$_2$O$_4$ NPs with 11 nm silica shell coupled to the action of the ORR-active mediator that ensures a high reversibility by promoting respectively an effective distribution of discharge products, and their full removal.

Characterization of the electrodes after the Li-air battery tests is important task for understanding of the electrochemical behaviour of the cathode catalysts in Li-air battery. In this respect, we characterized the electrodes by using SEM and FTIR at the end of cycling experiments and the results are presented by Figure 7. Figure 7a–b shows two representative SEM images of the electrodes comprising ZnFe$_2$O$_4$ with 11 nm silica shell. The display of toroid-like micron-size particles within the electrode is indicative of the formation of Li$_2$O$_2$ as main discharge products.[41] The formation of such a characteristic toroid-like Li$_2$O$_2$ particles has been reported for the Li-air batteries in the presence of non-carbonate electrolyte solvents
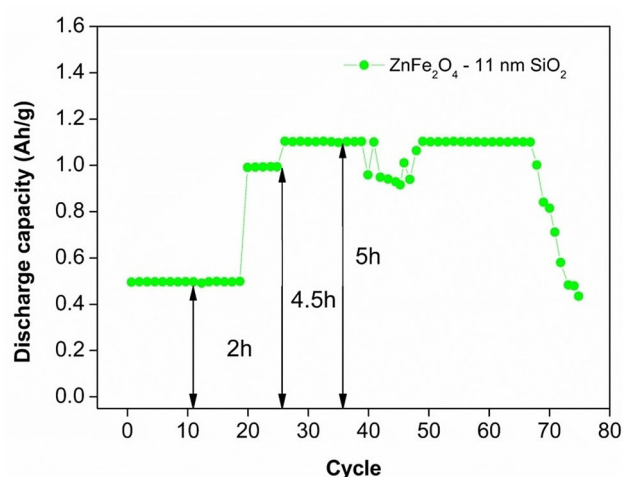
Figure 6. Cycling performance of electrodes comprising ZnFe$_2$O$_4$ NPs coated with an 11 nm silica shell at a discharge capacity limited to 1000 mAh g^{-1}. Discharge limited at 2 h (20 cycles), 4.5 h (6 cycles), and 5 h (50 cycles) at 0.1 mA/cm^2 with 0.1 M iodide in the electrolyte. The voltages were set at 2.5 V for discharging and 4.2 V for charging.
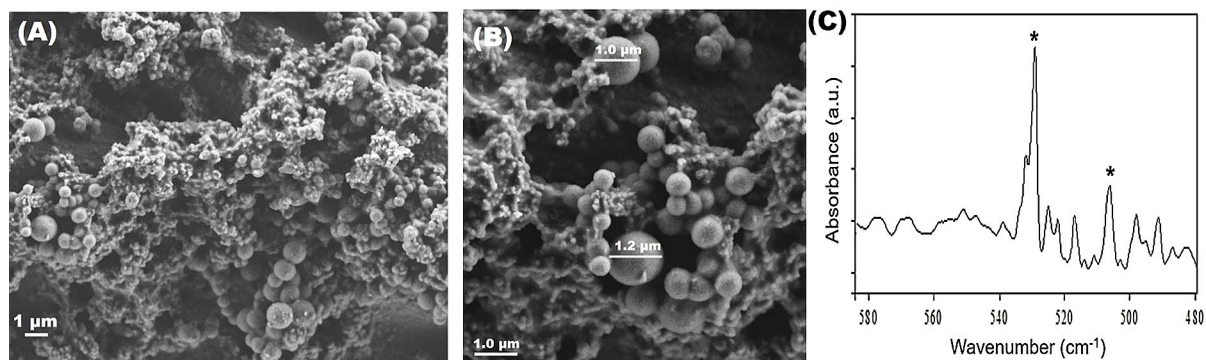
Figure 7. A,B) SEM images and C) FTIR spectrum of electrodes comprising ZnFe$_2$O$_4$ NPs with an 11 nm silica shell.

such as ethers used in this study.[42–44] The formation of Li$_2$O$_2$ as the main discharge products was also supported by the FTIR spectrum given in Figure 7c.

3. Conclusions

In summary, we have successfully synthesized colloidal ZnFe$_2$O$_4$ NPs and coated them with silica at three different thicknesses of 9, 11 and 13 nm. The effect of the silica coating for improved electrochemical performance of LABs is investigated. The primary discharge/charge capacities at 0.1 mA cm^{-2} were 3300, 4300, 6200 and 5000 mAh g^{-1} for uncoated ZnFe$_2$O$_4$ NPs, silica coated ZnFe$_2$O$_4$ NPs with 9 nm, 11 nm and 13 nm shell thickness, respectively. The overpotential is 0.5 V decreased by silica coating with a thickness of 11 nm, whereas there was no difference at other thicknesses. Cyclability with a discharge capacity of 1000 mAh g^{-1} was observed for at least 45 cycles with the silica coated ZnFe$_2$O$_4$ NPs with a layer thickness of 11 nm. This study is the first example for the use of silica coated ZnFe$_2$O$_4$ NPs with different shell-thickness. It can be concluded that silica coating is a convenient way for improving the electrochemical performance of ferrites as cathode catalysts for LABs.

Acknowledgement

Conflict of Interest

The authors declare no conflict of interest.

Keywords: catalysts · cathode material · lithium-air battery · silica coating · zinc ferrite

[1] P. Stevens, G. Toussaint, L. Puech, P. Vinatier, *ECS Trans.* **2013**, *50*, 1–11.
[2] N. Imanishi, A. C. Luntz, P. Bruce, The Lithium Air Battery: Fundamentals, Springer, New York, **2014**.
[3] D. Capsoni, M. Bini, S. Ferrari, E. Quartarone, P. D. Mustarelli, *J. Power Sources* **2012**, *220*, 253–263.
[4] Z. Jian, P. Liu, F. Li, P. He, X. Guo, M. Chen, H. Zhou, *Angew. Chem. Int. Ed.* **2014**, *53*, 442–446.
[5] E. Yoo, H. Zhou, *ACS Nano* **2011**, *5*, 3020–3026.
[6] L. Li, A. Manthiram, *Adv. Energy Mater.* **2014**, *4*, 1301795.
[7] L. Li, S.-H. Chai, S. Dai, A. Manthiram, *Energy Environ. Sci.* **2014**, *7*, 2630–2636.
[8] B. Gon Kim, H. Kim, S. Back, K.-W. Nam, J. Yung, Y. K. Han, J. W. Choi, *Sci. Rep.* **2014**, *4*, 4225.
[9] J.J. Wang, Y. L. Li, X. L. Sun, *Nano Energy* **2013**, *2*, 443–467.
[10] M. Sevim, T. Şener, Ö. Metin, *Int. J. Hydrogen Energy* **2015**, *40*, 10876–10882.
[11] T. Şener, E. Kayhan, M. Sevim, Ö. Metin, *J. Power Sources* **2015**, *288*, 36–41.
[12] Y. Li, K. Guo, J. Li, X. W. Dong, T. Yuan, X. W. Li, H. Yang, *ACS Appl. Mater. Interfaces* **2014**, *6*, 20949–20957.
[13] J. Li, M. Zou, W. Wen, Y. Zhao, Y. Lin, L. Chen, H. Lai, L. Guan, Z. Huang *J. Mater. Chem. A* **2014**, *2*, 10257–10262.
[14] W. Yin, Y. Shen, F. Zou, X. L. Hu, B. Chi, Y. H. Huang, *ACS Appl. Mater. Interfaces* **2015**, *7*, 4947–4954.
[15] Y. S. Mekonnen, K. B. Knudsen, J. S. G. Mýrdal, R. Younesi, J. Højberg, J. Hjelm, P. Norby, T. Vegge, *J. Chem. Phys.* **2014**, *140*, 121101.
[16] V. Timoshevskii, Z. Feng, K. H. Bevan, J. Goodenough, K. Zaghib, *Appl. Phys. Lett.* **2013**, *103*, 073901.
[17] W. Cho, S. M. Kim, J. H. Song, T. Yim, S. G. Woo, K. W. Lee, J. S. Kim, Y. J. Kim, *J. Power Sources* **2015**, *282*, 45–50.
[18] K. Cao, L. Jiao, Y. Liu, H. Liu, Y. Wang, H. Yuan, *Adv. Funct. Mater.* **2015**, *25*, 1082–1089.
[19] N. Shimoi, Y. Tanaka, *Electrochim. Acta* **2012**, *80*, 227–232.
[20] J. Shu, R. Ma, M. Shui, D. Wang, N. Long, Y. Ren, R. Zhang, J. Yao, X. Mao, W. Zheng S. Gao, *RSC Adv.* **2012**, *2*, 5806–5814.
[21] S. Evers, L. F. Nazar, *Acc. Chem. Res.* **2013**, *46*, 1135–1143.
[22] Y. Zhai, K. Xiao, J. Yu, J. Ding, *Electrochim. Acta* **2015**, *154*, 219–226.
[23] M. Kim, Y. S. Kim, Y.-G. Lee, J. H. Park, *RSC Adv.* **2013**, *3*, 16708–16713.
[24] J. Zhang, L. Yue, Q. Kong, Z. Liu, X. Zhou, C. Zhang, S. Pang, X. Wang, J. Yao, G. Cui, *J. Electrochem. Soc.* **2013**, *160*, A769-A774.
[25] S. M. Kang, M.-H. Ryou, J. W. Choi, H. Lee, *Chem. Mater.* **2012**, *24*, 3481–3485.
[26] C. Xia, M. Waletzko, K. Peppler, J. Janek, *J. Phys. Chem. C*, **2013**, *117*, 19897–19904.
[27] W. An, J. Fu, J. Su, L. Wang, X. Peng, K. Wu, Q. Chen, Y. Bi, B. Gao, X. Zhang, *J. Power Sources* **2017**, *345*, 227–236
[28] Z. L. Wang, D. Xu, J. J. Xu, X. B. Zhang, *Chem. Soc. Rev.* **2014**, *43*, 7746–7786.
[29] J. J. Xu, Z. L. Wang, D. Xu, F. Z. Menga, X. B. Zhang, *Energy Environ. Sci.* **2014**, *7*, 2213.
[30] Q. C. Liu, J. J. Xu, D. Xu, X. B. Zhang, *Nat. Commun.* **2015**, *6*, 7892.
[31] Q. C. Liu, L. Li, J. J. Xu, Z. W. Chang, D. Xu, Y. B. Yin, X. Y. Yang, T. Liu, Y. S. Jiang, J. M. Yan, X. B. Zhang, *Adv. Mater.* **2015**, *27*, 8095–8101.
[32] J. J. Xu, Z. W. Chang, Y. Wang, D. P. Liu, Y. Zhang, X. B. Zhang, *Adv. Mater.* **2016**, *28*, 9620–9628.
[33] Z. Chang, J. Xu, X. Zhang, *Adv. Energy Mater.* **2017**, 1700875

[34] D. Caruntu, Y. Remond, N. H. Chou, M. J. Jun, G. Caruntu, J. B. He, G. Goloverda, C. J. O'Connor, V. L. Kolesnichenko, *Inorg. Chem.* **2002**, *41*, 6137–6146.

[35] D. C. Lee, F. V. Mikulec, J. M. Pelaez, B. Koo, B. A. Korgel, *J. Phys. Chem. B* **2006**. *110*, 11160–11166

[36] B. J. Bergner, A. Schürmann, K. Peppler, A. Garsuch, J. Janek, *J. Am. Chem. Soc.* **2014**, *136*, 15054–15064.

[37] W. Kwak, D. Hirshberg, D. Sharon, H.-J Shin, M. Afri, J. B. Park, A. Garsuch, F. F. Chesneau, A. A. Frimer, D. Aurbach, Y. K. Sun, *J. Mater. Chem. A* **2015**, *3*, 8855–8864.

[38] I. L. Medrano, M. Olivares-Marín, R. Pinedo, I. Ruiz de Larramendi, T. Rojo, D. Tonti, *Electrochem. Commun.* **2015**, *59*, 24–27.

[39] K. S. Tan, A. C. Grimsdale, R. Yazami, *Sci. Rep.* **2017**, *7*, 6502.

[40] D. Wang, J. Zhou, J. Li, Y. Wang, H. Li. F. Gao, *ACS Sustainable Chem. Eng.* **2018**, *6*, 7339–7345.

[41] Y.-C. Lu, B. M. Gallant, D. G. Kwabi, J. R. Harding, R. R. Mitchell, M. S. Whittingh, Y. Shao-Horn, *Energy Environ. Sci.* **2013**, *6*, 750–768.

[42] Y.-C. Lu, D. G. Kwabi, K. P. C. Yao, J. R. Harding, J. Zhou, L. Zuin, Y. Shao-Horn, *Energy Environ. Sci.* **2011**, *4*, 2999–3007

[43] R. R. Mitchell, B. M. Gallant, C. V. Thompson, Y. Shao-Horn, *Energy Environ. Sci.* **2011**, *4*, 2952–2958.

[44] Z.-L. Wang, D. Xu, J.-J. Xu, L.-L. Zhang, X.-B. Zhang, *Adv. Funct. Mater.* **2012**, *22*, 3699–3705.